

A Three-Dimensional Angular Scattering Response Including Path Powers

Konstantinos Mammasis, *Member, IEEE*, Paolo Santi, *Member, IEEE*, Angelos Goulios, *Member, IEEE*.

Abstract

In this paper, the angular power spectrum exhibited under a three-dimensional (3-D) Gaussian scattering distribution at fixed observation points in space is investigated. Typically, these correspond to the mobile and base units, respectively. Unlike other spatial channel models, the derived model accounts for the distance to each scatterer from the observation point, and transforms distances into power values under the assumption of free-space propagation. The proposed 3-D spatial channel model follows a non-central approach in terms of the scatterer distribution in space, which means that the angular power field at the base unit need not be due to a scatterer distribution centered exactly at the mobile. Derivations are provided for the angular and power domains. An important finding is that, by conditioning the distance, the angular field reduces to the von-Mises Fisher distribution. Most importantly, this work provides a theoretical backup to the Gaussian angular power spectrum observed in radio propagation channel measurements, introducing a formal theoretical framework consistent with the experimental investigations found in literature. More specifically, our findings show that a Gaussian scatterer distribution in space gives rise to a Gaussian angular power spectrum and a Gaussian angular power density in the azimuth and elevations fields. By introducing the notion of distance into the framework, the proposed 3-D spatial channel model can be used to evaluate performance of current and future multi-element wireless communication networks.

Index Terms

Angular power scattering response, wireless spatial channel modeling, antenna arrays.

I. INTRODUCTION

Tri-dimensional analysis is an intriguing task for the purpose of spatial channel modeling and estimation. Restricting the direction of waves in the two-dimensional (2-D) plane reduces the mathematical complexity and makes the development and derivations of closed-form solutions relatively easy. However, the propagation channel is characterized by waves arriving from elevated regions, and not strictly from the azimuthal plane. This is especially true in micro and pico cell types of environments, where elevation of scatterers plays an important role. It is therefore important to analyze channel behavior including the effect of elevation, as pointed out also in some measurement-based studies – see, e.g., [1], [2].

Konstantinos Mammasis is a Researcher in the National Research Council of Italy, via Giuseppe Moruzzi 1, 56124, Pisa, Italy e-mail: konstantinos.mammasis@iit.cnr.it.

Paolo Santi is a Senior Researcher in the National Research Council of Italy, via Giuseppe Moruzzi 1, 56124, Pisa, Italy e-mail: paolo.santi@iit.cnr.it.

Angelos Goulios is a Lecturer in the Higher Technological Educational Institute of Greece, Department of Information and Communication Engineering, Terma Magnisias, 62124, Serres, Hellas.

Manuscript submitted on June 2011

The main goal of this work is to exploit and understand the effects of the spatial domain on the performance of the communication link. The interest in spatial domain is mainly due to the deployment of multi-element antenna systems in both the base and the mobile units in recent years. This is due to the potential benefits offered by these systems, which has also generated intense interest in developing accurate directional channel models. Yet, the performance of such systems is mainly evaluated under the assumption of 2-D propagation. This approach has contributed to the understanding of the azimuthal power spectrum, which is an important concept in spatial correlation, and ultimately in deriving information theoretic bounds for these systems. The angular power spectrum (APS) is a weighted version of the true scattering response, as affected by the presence of the antenna. In some cases, the effect of the antenna is removed from the measurements. This type of spectrum is typically inferred from measurements in practice, or it is otherwise derived by modeling the dependency between the angle of arrival of waves, the far-field radiation pattern of the antenna array, and the associated power density of the incoming waves. It is important to observe that, while the relationship between angle and power is *implicitly* dictated by the distance to each scattering point, to the best of the authors' knowledge existing works related to the APS do not *explicitly* account for the power loss due to the distance between the scatterer and observation point. Also, the scattering mechanism is not always linked to the observed APS, making its adoption ambiguous, since it lacks a physical interpretation. To exemplify this, consider the Laplacian-like APS, whose occurrence is typically observed in congested urban types of environments. While it is still not clear what scattering mechanism triggers the observance of this type of angular power spectrum from a geometry based stochastic modeling perspective, the research community has nonetheless used the Laplacian function for simulating the APS.

The connection between the APS and the true underlying distribution of scatterers is still under research for the 3-D case. Three-dimensional channel characterization has attracted increasing attention in recent years due to the potential benefits associated with the inclusion of the third dimension in the model, -see, e.g., [3], [4], among others. The authors in [3] developed a 3-D macrocell model to jointly analyze the spatial and temporal domain. The theoretical results presented are validated with the use of experimental data. However, the distribution of scatterers is confined in a 2-D circular disk, which clearly poses some limitations for the macrocellular scenario. In [4], Nawaz *et al.* use a geometry-based approach to jointly derive the angle and time of arrival statistics for both communication ends under the assumption of uniform scattering distribution confined in a semispheroid at the MS. A 3-D spheroid model is also developed in [5],

which allows scatterers to be distributed uniformly in a spheroid around the MS following a non-central approach. Various derivations are provided related to the angular distributions, whose standard deviation is allowed to vary in azimuth and elevation. The aforementioned works investigate the spatio-temporal nature of the channel and clearly have different targets and contributions from the 3-D model developed in here, where focus is shifted in the distribution of the power-angular domain in 3-D by following a non-central approach in terms of the scatter cluster at the mobile unit. The significance of 3-D models has been reinforced by the experimental research findings in [6], where the authors showed that 65% of the energy incident on a rectangular synthetic antenna array had an elevation larger than 10° . Additionally, in [7] the authors report that 90% of the energy is confined within an elevation range of 0° to 40° . In [1], a spherical outdoor to indoor power spectrum model is developed for the MS, where the necessity of including the third dimension is further emphasized. Finally, in [8] the experimental results confirmed that for a small hand-held antenna device (MS) having low directivity, the contribution of multipaths arriving from higher elevation regions is significant. A key finding of [8] is the importance of the diffracted components from the rooftop edges and other objects (e.g. high lamp posts) that arrived with elevations as high as 60° . It is evident that in these conditions the incoming power angular spectra can be fully characterized only using a 3-dimensional model that considers also the effect of elevation. We want to stress that a 3-dimensional model proves useful also in case handsets are equipped with 2-D antenna arrays – as it is the case with current technology, at the very least to get an estimate of how well a 2-D array performs as compared to an optimal 3-D topology.

In the 2-D case, the authors in [9] observed through experimental investigations that a Gaussian distribution in angle of arrival (AoA) gives rise to a Laplacian-like power azimuth spectrum (PAS). The Laplacian function was also considered in [10] for modeling the AoA of multipaths, which may be attributed to the congested environment in this case. In general, many different propositions of AoA and APS have been made considering different scatterer distributions but mainly Gaussian, von Mises and uniform. Therefore, the shape of scattering region, the density of the scatterers within it, the location of scatterers in space, and the power emitted by each scatterer are important aspects in the derivation of the corresponding APS. Starting from a Gaussian scattering density around the mobile station (MS), Janaswamy in [11] derived the corresponding AoA and APS as seen by the base station (BS). Joint time of arrival and AoA statistics were also derived in [12] assuming uniform distribution of scatterers. Therefore, in [11], [12] the authors derived the spatial channel statistics in accordance with a given

geometrical arrangement of scatterers. However, both models consider a 2-D geometry. Further, in both cases a formal characterization of the APS was not given, while attention was concentrated towards the joint angle and time of arrival statistics in 2-D.

In this paper, a novel theoretical framework for 3-D channel characterization under the Gaussian scatterer assumption is proposed. The work begins by modeling the overall scattering response in 3-D as a function of distance and angle to the observation point. The presented approach allows positioning the center of the cluster at an arbitrary distance from the observation point, which widens the model's applicability from macrocell to microcell and possibly to picocell scenarios. The Gaussian scattering assumption is of particular interest because it has been observed experimentally in [9]. Starting from this Gaussian scattering distribution, the corresponding distance-dependent AoA statistics at the observation point are derived. Dependence on distance of the AoA statistics motivated us to use the term *angular distance scattering response* (DASR), which corresponds to the joint probability density function (PDF) of AoA and distance. The methodology and derivations reveal a von Mises Fisher (vMF) AoA spectrum when conditioning the joint density function at a particular distance value. Later in the paper, power angular statistics are derived from the distribution of distances through the super-imposition of free-space propagation, which allows one to fully characterize the 3-D *angular power scattering response* (PASR). To the best of the authors' knowledge, a formal characterization of the 3-D PASR has not been considered elsewhere in the literature. The foreseen target of this work is an accurate estimation of the antenna response under a realistic and well-defined angular power field. The proposed model can be applied for the optimization of the antenna response in order, e.g., to minimize the correlation experienced between the elements of a multi-antenna system. This essentially offers some degree of pattern diversity to the system by orthogonalizing the embedded patterns.

The rest of this paper is organized as follows: in Section II the 3-D scatter model and methodology are analyzed. Section III details the transformation of the 3-D Gaussian scattering density from Cartesian to the spherical co-ordinate system. In Section IV and V the derivations of the distance and angular distributions, respectively, are presented. Section VI presents a procedure to transform the distance distribution into a power distribution. Power values are then associated with each incoming angle in order to weight the angle of arrival spectrum in Section VII-B. Finally, the conclusions of this work are drawn in Section VIII.

II. 3-D SCATTER MODEL AND METHODOLOGY

The geometric model of reference is reported in Figure 1: a cluster of scatterers is randomly distributed around a point in the plane – named the *center of gravity* (CoG for short) in the following – according to a tri-variate Gaussian distribution. A receiver node ρ_1 is located in another point of the plane, assumed to be the origin of the Euclidean plane, and named the *observation point* in the following. Deterministic elements in the geometry are the position $\rho_1 = (0, 0, 0)$ of the receiver, and the position $CoG = (x_0, y_0, z_0)$ of the CoG. Random elements in the geometry are the positions of specific scatterers, represented as gray circles in Figure 1. Once again it should be stressed that, differently from [11] (which, however, was a 2-D model), this work does not assume that the scatter CoG is co-located with ρ_1 ; instead, the CoG is located at an arbitrary position (x_0, y_0, z_0) in the plane, as defined by vector Ω_o reported in Figure 1. To keep the model tractable, though, we make a simplifying assumption concerning the distribution of scatterers around the CoG, which is assumed to be independent and symmetric in the three considered dimensions; i.e., a single value of the standard deviation σ is used to disperse scatterers around the CoG in the three dimensions.

Our interest in this paper is in deriving a model predicting the PASR observed at the observation point. It is important to note that the derived expression is a *distribution* and not a spectrum (PAS). In other words, the derived PASR allows determining, for each incoming azimuthal direction φ , elevation ϑ , and possible power value P , the probability density of observing exactly power P incoming from direction (φ, ϑ) at a generic instant of time t . On the other hand, the PAS characterizes the *average* amount of power incoming from (φ, ϑ) , where averaging is done in the temporal dimension. Turning the PASR derived herein into the traditional notion of PAS is then an exercise amounting to derive, for each given direction (φ, ϑ) , the *expected* amount of power incoming from (φ, ϑ) .

Note that two random quantities need to be derived in order to estimate the PASR: given an azimuth, elevation pair (φ, ϑ) , the *density* of scatterers observed at ρ_1 along direction (φ, ϑ) needs to be characterized – i.e., the angular scatterer density, and the *density of power* received at ρ_1 incoming from a scatterer along direction (φ, ϑ) , which signifies the scatterer power density (see Figure 1). The composition of these two densities allows us to derive the desired PASR.

It is important to observe that, in order to estimate the scatterer power density – i.e., the pdf of the random variable $P_{\rho_1, \varphi, \vartheta}$ denoting the power received at ρ_1 incoming from a scatterer along direction (φ, ϑ) – two quantities need to be derived: *i*) the pdf of the *distance* between ρ_1 and a scatterer along direction

(φ, ϑ) (denoted $\|\Omega_{\rho_1,sc}\|$ in Figure 1), and *ii*) the pdf of the *distance* between a scatterer along direction (φ, ϑ) and the transmitter ρ_2 (denoted $\|\Omega_{\rho_2,sc}\|$ in Figure 1). In fact, if *i*) and *ii*) are known, conventional path loss models can be used to convert *ii*) into an estimate of the amount of power emitted by a scatterer as a response to transmission from ρ_2 , and to convert *i*) into an estimate of the amount of power received at ρ_1 .

Note that, while distance distribution *i*) is relatively easy to obtain since the distance $\|\Omega_o\|$ between ρ_1 and the CoG is a deterministic element of the reference geometry, deriving *ii*) is relatively more complex. Two approaches can be undertaken here: in the first approach, the position of transmitter ρ_2 is not known. Our interest in this case is deriving the PASR observed at ρ_1 conditioned on a specific distance d between ρ_2 and CoG. In this situation, *ii*) can be derived along the same lines as *i*), by simply substituting $\|\Omega_o\|$ with d . In other words, lengths of vectors $\|\Omega_{\rho_1,sc}\|$ and $\|\Omega_{\rho_2,sc}\|$ in Figure 1 can be considered as independent random variables, and this scenario is then called *independent case* in the following. In the second approach, the position of transmitter ρ_2 is known, hence vector $\|\Omega_d\|$ is another deterministic element in the geometry. The analysis of this case is more complex than the previous one, since now lengths $\|\Omega_{\rho_1,sc}\|$ and $\|\Omega_{\rho_2,sc}\|$ are correlated random variables. More specifically, given $\|\Omega_{\rho_1,sc}\|$, the value of $\|\Omega_{\rho_2,sc}\|$ can be computed applying the law of cosines to triangle (ρ_1, ρ_2, S) , where angle γ is a random variable introducing a non-trivial correlation between $\|\Omega_{\rho_1,sc}\|$ and $\|\Omega_{\rho_2,sc}\|$. This scenario is called *correlated case* in the following. The derivation of the power angular scattering response under the correlated case is left for future work.

Fig. 1 HERE

III. TRANSFORMATION OF THE 3-D GAUSSIAN SCATTERING DENSITY

The derivation of the DASR as observed at an arbitrary point in space has to account for the distances and directions of the corresponding vectors. The adoption of the widely used Gaussian model provides a good trade-off between complexity and intuition of the problem in consideration. Scatterers are distributed around a CoG located at (x_o, y_o, z_o) under the constrained¹ multivariate Gaussian distribution, with mean μ and standard deviation σ . The concentration of scatterers around the mean vector x_o, y_o, z_o is defined through the parameter σ . Independence is preserved, allowing the joint density function $f(x, y, z)$ to be written as the product of the individual marginal densities $f(x)$, $f(y)$ and $f(z)$. Hence, the distance of

¹The term “constrained” in here implies no correlation between x , y and z , implying that the three components of the vector representing a scatterer’s position in space are distributed independently.

each directional vector to a scatterer is given by $\|\mathbf{\Omega}_{\rho_1,sc}\| = (x^2 + y^2 + z^2)^{1/2}$, and its associated orientation by an azimuthal angle $\varphi = \arctan(y/x)$ and a co-latitude angle $\vartheta = \arccos(z/\|\mathbf{\Omega}_{\rho_1,sc}\|)$. To proceed, let the Gaussian density function for a random variable X be expressed as follows

$$f_X(x) = \frac{1}{\sqrt{2\pi}\sigma} e^{-(x-x_o)/2\sigma^2}, -\infty \leq x \leq \infty, \quad (1)$$

which suggests that the product of the marginal densities in accordance with (1) results in

$$f_{XYZ}(x, y, z) = \frac{1}{(2\pi)^{3/2}\sigma^3} e^{-[(x-x_o)^2 + (y-y_o)^2 + (z-z_o)^2]/2\sigma^2}. \quad (2)$$

This function strictly characterizes the scatterer locations in space, but it does not reveal any angular information at the observation unit. In order to obtain the desired DASR in 3-D, a transformation of the corresponding co-ordinate system is required.

Transforming into the more convenient spherical co-ordinate system allows us to view this problem from the angular domain. After simple algebraic manipulation and considering the Jacobian of the transformation, the joint density function with respect to the spherical co-ordinate system becomes [13]

$$f_{R\Theta\Phi}(\|\mathbf{\Omega}\|, \vartheta, \varphi) = f_{XYZ}(x, y, z) \frac{\partial(x, y, z)}{\partial(\|\mathbf{\Omega}_{\rho_1,sc}\|, \vartheta, \varphi)}, \quad (3)$$

with

$$\begin{aligned} x &= \|\mathbf{\Omega}_{\rho_1,sc}\| \sin \vartheta \cos \varphi, y = \|\mathbf{\Omega}_{\rho_1,sc}\| \sin \vartheta \sin \varphi, z = \|\mathbf{\Omega}_{\rho_1,sc}\| \cos \vartheta, \\ x_o &= \|\mathbf{\Omega}_o\| \sin \vartheta_o \cos \varphi_o, y_o = \|\mathbf{\Omega}_o\| \sin \vartheta_o \sin \varphi_o, z_o = \|\mathbf{\Omega}_o\| \cos \vartheta_o. \end{aligned}$$

Note that $\|\mathbf{\Omega}_o\|$ denotes the distance of the mean directional vector $\mathbf{\Omega}_o$, and ϑ_o, φ_o are the associated azimuth and elevation angles of this vector. From (2) and (3), the joint density function in terms of the new random variables may be written as follows:

$$\begin{aligned} f_{R\Theta\Phi}(\|\mathbf{\Omega}_{\rho_1,sc}\|, \vartheta, \varphi) &= \frac{\|\mathbf{\Omega}_{\rho_1,sc}\|^2 \sin \vartheta}{(2\pi)^{3/2}\sigma^3} e^{\|\mathbf{\Omega}_{\rho_1,sc}\|^2 \sin^2 \vartheta \cos^2 \varphi + \|\mathbf{\Omega}_o\|^2 \sin^2 \vartheta_o \cos^2 \varphi_o - 2\|\mathbf{\Omega}_{\rho_1,sc}\|\|\mathbf{\Omega}_o\| \sin \vartheta \cos \varphi \sin \vartheta_o \cos \varphi_o / 2\sigma^2} \times \\ &\times e^{\|\mathbf{\Omega}_{\rho_1,sc}\|^2 \sin^2 \vartheta \sin^2 \varphi + \|\mathbf{\Omega}_o\|^2 \sin^2 \vartheta_o \sin^2 \varphi_o - 2\|\mathbf{\Omega}_{\rho_1,sc}\|\|\mathbf{\Omega}_o\| \sin \vartheta \sin \varphi \sin \vartheta_o \sin \varphi_o / 2\sigma^2} \\ &\times e^{\|\mathbf{\Omega}_{\rho_1,sc}\|^2 \cos^2 \vartheta + \|\mathbf{\Omega}_o\|^2 \cos^2 \vartheta_o - 2\|\mathbf{\Omega}_{\rho_1,sc}\|\|\mathbf{\Omega}_o\| \cos \vartheta \cos \vartheta_o / 2\sigma^2} \\ &= \frac{\|\mathbf{\Omega}_{\rho_1,sc}\|^2}{(2\pi)^{3/2}\sigma^3} e^{-\{\|\mathbf{\Omega}_{\rho_1,sc}\|^2 + \|\mathbf{\Omega}_o\|^2 - 2\|\mathbf{\Omega}_{\rho_1,sc}\|\|\mathbf{\Omega}_o\|[\sin \vartheta \sin \vartheta_o \cos(\varphi - \varphi_o) + \cos \vartheta \cos \vartheta_o]\} / 2\sigma^2} \sin \vartheta \Rightarrow \\ f_{R\Theta\Phi}(\|\mathbf{\Omega}_{\rho_1,sc}\|, \vartheta, \varphi) &= \frac{\|\mathbf{\Omega}_{\rho_1,sc}\|^2}{(2\pi)^{3/2}\sigma^3} e^{-(\|\mathbf{\Omega}_{\rho_1,sc}\|^2 + \|\mathbf{\Omega}_o\|^2) / 2\sigma^2} e^{\|\mathbf{\Omega}_{\rho_1,sc}\|\|\mathbf{\Omega}_o\| / \sigma^2 [\sin \vartheta \sin \vartheta_o \cos(\varphi - \varphi_o) + \cos \vartheta \cos \vartheta_o]} \sin \vartheta. \end{aligned} \quad (4)$$

This function represents the so-called distance-dependent AoA spectrum as observed at ρ_1 . Under this

representation, the DASR at ρ_1 is taken with respect to the center of gravity of the scatterers in its vicinity, as depicted in Fig. 1.

IV. ANALYSIS OF THE DISTANCE DISTRIBUTION

To investigate the properties of the joint distribution function $f_{R,\Theta,\Phi}$, a decomposition into the distance and angular domains is required. In this section, emphasis is given in the distribution of distances. To derive the distribution of distances $f(\|\Omega_{\rho_1,sc}\|)$, ignoring any constraints imposed by the amplitude of Ω_o , integration is performed (4) with respect to the angular domain:

$$\begin{aligned}
 f(\|\Omega_{\rho_1,sc}\|; \|\Omega_o\|, \sigma) &= \iint_{\mathbb{S}^2} f(\|\Omega_{\rho_1,sc}\|, \vartheta, \varphi) d\vartheta d\varphi \\
 &= \frac{\|\Omega_{\rho_1,sc}\|^2}{(2\pi)^{3/2}\sigma^3} e^{-(\|\Omega_{\rho_1,sc}\|^2 + \|\Omega_o\|^2)/2\sigma^2} \iint_{\mathbb{S}^2} e^{\|\Omega_{\rho_1,sc}\|\|\Omega_o\|/2\sigma^2 [\sin\vartheta \sin\vartheta_o \cos(\varphi - \varphi_o) + \cos\vartheta_o \cos\vartheta]} \times \\
 &\hspace{20em} \times \sin\vartheta d\vartheta d\varphi \\
 &= \frac{\|\Omega_{\rho_1,sc}\|^2}{(2\pi)^{3/2}\sigma^3} e^{-(\|\Omega_{\rho_1,sc}\|^2 + \|\Omega_o\|^2)/2\sigma^2} \Gamma(3/2) (\|\Omega_{\rho_1,sc}\|\|\Omega_o\|/2\sigma^2)^{-1/2} I_{1/2}(\|\Omega_{\rho_1,sc}\|\|\Omega_o\|/\sigma^2) \\
 &= \frac{\sqrt{2}\|\Omega_{\rho_1,sc}\| \sinh(\|\Omega_{\rho_1,sc}\|\|\Omega_o\|/\sigma^2)}{\sqrt{\pi}\sigma\|\Omega_o\|} e^{-(\|\Omega_{\rho_1,sc}\|^2 + \|\Omega_o\|^2)/2\sigma^2}, \quad \|\Omega_{\rho_1,sc}\| \geq 0,
 \end{aligned} \tag{5}$$

where $\|\Omega_o\|$ is a shape parameter, σ controls dispersion of scatterers, and \mathbb{S}^2 denotes integration over spherical co-ordinates. Note the properties of the special functions $\Gamma(n)$ and $I(n)$ used during this derivation:

$$\begin{aligned}
 I_{1/2}(\|\Omega_{\rho_1,sc}\|\|\Omega_o\|/\sigma^2) &= \frac{1}{(\pi\|\Omega_{\rho_1,sc}\|\|\Omega_o\|/2\sigma^2)^{1/2} (1/\sinh(\|\Omega_{\rho_1,sc}\|\|\Omega_o\|/\sigma^2))}, \\
 \Gamma(3/2) &= \sqrt{\pi/2}.
 \end{aligned}$$

The function $\Gamma(n)$ denotes the Gamma function of argument n , while the function $I_{1/2}(n)$ denotes the Modified Bessel functions of the first kind and half-integer order [14]. Note also that reference to the random variables has been dropped to simplify notation.

An evaluation of the derived distribution in (5) reveals two types of behavior depending on the ratio $\|\Omega_o\|/\sigma$. Figure 2 shows two cases where the magnitude of Ω_o gradually increases. Observe that the distribution of distances obtains a Gaussian-like shape for large $\|\Omega_o\|/\sigma$. Instead, for lower values of $\|\Omega_o\|$ the distribution is asymmetrical to the mean and in particular it is left-skewed². Note that the

²Relationship with other distributions: The nature of the derived distribution is similar to the Rayleigh's characteristics for the 2D vector case, where the magnitude of the vector is related to its directional components. If the individual components of this vector are analyzed such that each one of them is independent and uncorrelated from the rest, then the overall vector's magnitude will be Rayleigh distributed.

evaluation of (5) has been superimposed with the fit assessment of the next section. In the next section, a goodness-of-fit test indicates the distributions that most closely match the two observed shapes.

A. Limiting Forms of the Derived Distribution of Distances

To better characterize the shape of the distribution in (5) for the limiting cases of small and large $\|\Omega_o\|$, a goodness-of-fit assessment test was performed using rejection sampling [15]. It was observed that for small mean distances the Nakagami distribution provides an excellent fit to the distance distribution, while for larger mean distances the Gaussian distribution is more appropriate. The goodness-of-fit becomes evident in Fig. 2. This makes the proposition of these two models suitable for a wide range of mean distances from the observation point. More specifically, if the scatterers lie close to the observation point their associated distances $\|\Omega_\rho\|$ will resemble a Nakagami distribution, i.e. $\|\Omega_\rho\| \sim \text{Nakagami}(\bar{\mu}, \omega)$; if the scatterers are relatively distant from the observation point, the Gaussian distribution of distances is more appropriate, i.e. $\|\Omega_\rho\| \sim N(\mu', \sigma')$. Parameters of the Nakagami and Gaussian approximation of the distance distribution for close and distant scatter cluster, respectively, have been numerically evaluated in Fig. 2. Giving explicit expressions of parameters $\bar{\mu}, \omega, \mu'$ and σ' as a function of distance $\|\Omega_o\|$ and concentration σ is beyond the scope of this paper, and is left for future work.

It is important to observe that the transition between the Nakagami and Gaussian regime of the distance distribution occurs when $\|\Omega_\rho\|$ is about 2σ . The range of distances in which the Nakagami distribution provides a good fit is displayed as the *close-in region*, while for the Gaussian distance distribution is called the *far-away region*.

To explain the different regimes of distance distributions, consider Fig. 3, which represents a 2-D geometry for simplicity. Consider a thin annulus of radius r centered at ρ_1 . If ρ_1 is in the close-in region and r is relatively small, then scatterers can lie with non-negligible probability not only in the “forward” part of the annulus, but also in its “backward” part (see Fig. 3). If the value of r increases, though, the probability of finding scatterers in the “backward” part of the annulus becomes zero, and scatterers can be found with non-negligible probability only in a fraction of the “forward” part of the annulus. The fact that scatterers can be found with non-negligible probability in the “backward” part of the annulus only when r is relatively small is at the origin of the left-skewness of the distance distribution when ρ_1 lies in the close-in region. On the other hand, when ρ_1 lies in the far-away region the probability of finding scatterers in the “backward” part of the annulus is negligible for all values of r , and the distance distribution becomes symmetric.

Fig. 2 HERE

Fig. 3 HERE

1) *Characterizing the Mean Distance:* To complete the characterization procedure of the distance PDF it becomes necessary to obtain the first and second order moment of the derived distribution. The mean value of the distance variable $\|\Omega_{\rho_1,sc}\|$ may be found as follows:

$$\mathbb{E} [\|\Omega_{\rho_1,sc}\|] = \int_0^\infty \|\Omega_{\rho_1,sc}\| f(\|\Omega_{\rho_1,sc}\|) d\|\Omega_{\rho_1,sc}\|. \quad (6)$$

Derivation:

$$\begin{aligned} \mathbb{E} [\|\Omega_{\rho_1,sc}\|] &= \int_0^\infty \frac{\sqrt{2}\|\Omega_{\rho_1,sc}\|^2 \sinh(\|\Omega_{\rho_1,sc}\|\|\Omega_o\|/\sigma^2)}{\sqrt{\pi}\sigma\|\Omega_o\|} e^{-(\|\Omega_{\rho_1,sc}\|^2 + \|\Omega_o\|^2)/2\sigma^2} d\|\Omega_{\rho_1,sc}\| \\ &= \frac{\sqrt{2}}{2\sqrt{\pi}\sigma\|\Omega_o\|} e^{-\|\Omega_o\|^2/2\sigma^2} \int_0^\infty \left(e^{\frac{\|\Omega_{\rho_1,sc}\|\|\Omega_o\|}{\sigma^2}} - e^{-\frac{\|\Omega_{\rho_1,sc}\|\|\Omega_o\|}{\sigma^2}} \right) \|\Omega_{\rho_1,sc}\|^2 e^{-\|\Omega_{\rho_1,sc}\|^2/2\sigma^2} d\|\Omega_{\rho_1,sc}\| \\ &= \frac{\sqrt{2}}{\sqrt{\pi}\sigma\|\Omega_o\|} e^{-\|\Omega_o\|^2/2\sigma^2} \left[\sigma^2\|\Omega_o\| + e^{\|\Omega_o\|^2/2\sigma^2} \sigma \frac{\sqrt{2\pi}}{2} (\|\Omega_o\|^2 + \sigma^2) \text{Erf} \left[\frac{\|\Omega_o\|}{\sqrt{2}\sigma} \right] \right] \\ &= \frac{\sqrt{2}}{\sqrt{\pi}} \sigma e^{-\|\Omega_o\|^2/2\sigma^2} + \frac{\|\Omega_o\|^2 + \sigma^2}{\|\Omega_o\|} \text{Erf} \left[\frac{\|\Omega_o\|}{\sqrt{2}\sigma} \right], \end{aligned} \quad (7)$$

where the classic identity of the hyperbolic sine, i.e. $\sinh x = 1/2(e^x - e^{-x})$, has been used and $\text{Erf}\{\cdot\}$ denotes the error function. As seen from the formula, the mean distance value of the random variable $\|\Omega_{\rho_1,sc}\|$ is not equal to $\|\Omega_o\|$, and it is in fact related to the dispersion parameter. To further analyze the behavior of the first order moment of the distance distribution, the limit of $\mathbb{E} [\|\Omega_{\rho_1,sc}\|]$ as $\|\Omega_o\| \rightarrow \infty$ is derived:

$$\begin{aligned} \lim_{\|\Omega_o\| \rightarrow +\infty} \mathbb{E} [\|\Omega_{\rho_1,sc}\|] - \|\Omega_o\| &= \lim_{\|\Omega_o\| \rightarrow +\infty} \frac{\sqrt{2}}{\sqrt{\pi}} \sigma e^{-\|\Omega_o\|^2/2\sigma^2} + \frac{\|\Omega_o\|^2 + \sigma^2}{\|\Omega_o\|} \text{Erf} \left[\frac{\|\Omega_o\|}{\sqrt{2}\sigma} \right] - \|\Omega_o\| \\ &= \lim_{\|\Omega_o\| \rightarrow +\infty} \frac{\sqrt{2}}{\sqrt{\pi}} \sigma e^{-\|\Omega_o\|^2/2\sigma^2} + \lim_{\|\Omega_o\| \rightarrow +\infty} \frac{\|\Omega_o\|^2 + \sigma^2}{\|\Omega_o\|} \text{Erf} \left[\frac{\|\Omega_o\|}{\sqrt{2}\sigma} \right] - \\ &\quad - \lim_{\|\Omega_o\| \rightarrow +\infty} \|\Omega_o\| \\ &= \lim_{\|\Omega_o\| \rightarrow +\infty} \frac{\|\Omega_o\|^2 + \sigma^2}{\|\Omega_o\|} \lim_{\|\Omega_o\| \rightarrow +\infty} \text{Erf} \left[\frac{\|\Omega_o\|}{\sqrt{2}\sigma} \right] - \lim_{\|\Omega_o\| \rightarrow +\infty} \|\Omega_o\| = 0. \end{aligned} \quad (8)$$

This result is due to the exponential term vanishing to zero as $\|\Omega_o\| \rightarrow \infty$, and also due to the property of the error function, i.e. $\lim_{x \rightarrow +\infty} \text{Erf}(x) = 1$. It follows directly that the mean of the random variable converges to the shape parameter $\|\Omega_o\|$ as the latter tends to infinity. This can be seen, for instance, in Fig 2: while for small values of $\|\Omega_o\|$ the expected value of the distribution is much larger than $\|\Omega_o\|$

(upper plot), it becomes very close to $\|\Omega_o\|$ when $\|\Omega_o\|$ becomes larger (bottom plot).

Similarly, the variance of the random variable may be found by considering the expectation $E[\|\Omega_{\rho_1,sc}\| - E[\|\Omega_{\rho_1,sc}\|]]^2$, with:

$$E[\|\Omega_{\rho_1,sc}\| - E[\|\Omega_{\rho_1,sc}\|]]^2 = -\frac{2\sqrt{2\pi}e^{-\|\Omega_o\|^2/2\sigma^2}\sigma(\|\Omega_o\|^2 + \sigma^2)\text{Erf}\left[\frac{\|\Omega_o\|}{\sqrt{2}\sigma}\right]}{\|\Omega_o\|\pi} - \frac{(\|\Omega_o\|^2 + \sigma^2)^2\text{Erf}\left[\frac{\|\Omega_o\|}{\sqrt{2}\sigma}\right]^2}{\|\Omega_o\|^2} - \frac{2\sigma^2e^{-\|\Omega_o\|^2/\sigma^2}}{\pi} + (\|\Omega_o\|^2 + 3\sigma^2). \quad (9)$$

The difference of the second-order moment obtained in (9) and the true variance of the distribution tends to zero as $\|\Omega_o\| \rightarrow \infty$. Therefore the following limit applies:

$$\lim_{\|\Omega_o\| \rightarrow +\infty} E[\|\Omega_{\rho_1,sc}\| - E[\|\Omega_{\rho_1,sc}\|]]^2 \rightarrow \sigma^2, \quad (10)$$

indicating that increasing the parameter $\|\Omega_o\| \rightarrow +\infty$, the second-order moment converges to the variance σ^2 of the scattering distribution. Therein, the standard deviation behaves identically, and it approaches its true value as the shape parameter $\|\Omega_o\|$ approaches infinity. This is reasonable since at low mean distance values the distribution of distances is asymmetrical to the mean.

2) *The Interplay of Standard Deviation and Distance:* The transformation of the scattering function to the spherical co-ordinate system and the introduction of new parameters in the density function establishes the need for clarifying the definition of standard deviation of the transformed distance density. In the Cartesian co-ordinate system, the standard deviation was solely determined by σ . After transformation, the parameter σ is not sufficient to express the dispersion of scatterers around the mean vector Ω_o . As revealed in (7) and (9), the first and second order moments of the random variable denoting distance from a random scatterer are dependent on the length of Ω_o and on the parameter σ . Increasing the mean distance Ω_o has a profound effect on the distribution of scattering points, altering its shape. However, the question that naturally arises is the change introduced in σ with successive increments of the mean distance with respect to the origin. Intuitively, the standard deviation σ remains unchanged by increasing the length of the mean vector Ω_o . Consequently, in the limit of the mean distance increasing indefinitely, a zero standard deviation at the observation point cannot be obtained. However, if one considers the normalized dispersion, defined as $\hat{\sigma} = \sigma/\|\Omega_o\|$, the situation is different.

In the limit of $\hat{\sigma} = \sigma/\|\Omega_o\| \rightarrow 0$, the distribution $f(\|\Omega_{\rho_1,sc}\|; \|\Omega_o\|, \sigma)$ converges to a Dirac-Delta function δ_f , where the peak of the Dirac function depends on the value of the two parameters. Alternatively,

$f(\|\Omega_{\rho_1,sc}\|)$ approaches zero $\forall \|\Omega_{\rho_1,sc}\|, \|\Omega_{\rho_1,sc}\| \neq \|\Omega_o\|$. Convergence to Dirac-Delta function can be formally proven by showing that the limit of $f(\|\Omega_{\rho_1,sc}\|; \|\Omega_o\|, \sigma)$ as $\sigma \rightarrow 0$ tends to infinity for $\|\Omega_{\rho_1,sc}\| = \|\Omega_o\|$. The following applies:

$$\lim_{\sigma \rightarrow 0} f(\|\Omega_{\rho_1,sc}\| = \|\Omega_o\|; \|\Omega_o\|, \sigma) = \infty.$$

To fully assimilate the effect of Ω_o on the joint distribution, focus should preferably be shifted to the angular distribution. Intuitively, the concentration of angles should increase as the length of Ω_o increases. To confirm this, the general distribution of angles is derived in the forthcoming section.

V. 3-D ANGULAR SCATTERING RESPONSE

In this section, the angular distribution of incoming waves under the 3-D Gaussian scatter density model is examined. The derived distribution expresses the true angular scattering response prior the introduction of any power dependency. As shown in the following, the concentration of angles increases as the length of the mean distance vector increases. Further, it is shown that the distribution of angles follows the vMF model by appropriate conditioning on each scatterer's distance to the observation unit. The general form of the distribution of angles is obtained by solving the integral with respect to the spatial domain in (4):

$$\begin{aligned} f(\vartheta, \varphi; \|\Omega_o\|, \sigma) &= \int_0^\infty f(\|\Omega_{\rho_1,sc}\|, \vartheta, \varphi) d\|\Omega_{\rho_1,sc}\| \\ &= \frac{1}{(4\pi)^{3/2}\sigma^2} e^{-\|\Omega_o\|^2/2\sigma^2} \left(2\|\Omega_o\|\sigma \cos \gamma + e^{\|\Omega_o\|^2 \cos^2 \gamma/2\sigma^2} \sqrt{2\pi} (\sigma^2 + \|\Omega_o\|^2 \cos^2 \gamma) \right) \\ &\quad \left(1 + \text{Erf} \left[\frac{\|\Omega_o\| \cos \gamma}{\sqrt{2}\sigma} \right] \right) \sin \vartheta. \end{aligned} \tag{11}$$

This is the general form of the distribution of angles for a Gaussian distribution of scatterers in 3-D³. The distribution of angles is a function of ϑ and φ , as expressed through $\cos \gamma = \sin \vartheta \sin \vartheta_o \cos(\varphi - \varphi_o) + \cos \vartheta_o \cos \vartheta$. It can be shown that, as intuition suggests, increments in the length of Ω_o cause an increase in the concentration of angles. The functional form of Ω_o is illustrated in Fig. 4. To formally show the above described behavior of angular concentration for increasing $\|\Omega_o\|$, it suffices to consider $\cos \gamma$ as

³Note that the distribution of angles has a common variance, i.e. azimuth and elevation variance is equal. This is carried over through the initial assumption of x, y, z being independently distributed. Admittedly, the equal variance assumption of the azimuth and elevation is not applicable in all cases, since elliptical clusters may be encountered. However, as shown in [16], [17] the difference in terms of the experienced correlation between two adjacent elements is insignificant for the same number of clusters—as these were identified through two different probabilistic model-based clustering approaches. Hence, modeling azimuth and elevation with equal variances is not unrealistic, although as shown, elliptically shaped clusters decorrelate the channel statistics. The key point here is that finding the cluster dispersion in azimuth and elevation is very much dependent on the clustering methodology used. Reminiscing the cited findings, the Fisher-Bingham distribution exhibits elliptical density contours, in contrast to the vMF's strict circular probability contours. The main disadvantage associated with both the vMF and FB5 models is that the variable distance is not treated as random, which would certainly complete the approach and make it more attractive, at least from a geometry-based stochastic modeling perspective.

the random quantity, and derive the first order moment as follows:

$$\mathbb{E}[\cos \gamma] = 2\pi \int_{-1}^1 \cos \gamma f(\cos \gamma; \|\Omega_o\|, \sigma) d(\cos \gamma) = e^{-\|\Omega_o\|^2/2\sigma^2} \sqrt{\frac{2}{\pi}} \sigma \|\Omega_o\|^{-1} + \left(1 - \frac{\sigma^2}{\|\Omega_o\|^2}\right) \text{Erf} \left[\frac{\|\Omega_o\|}{\sqrt{2}\sigma} \right]. \quad (12)$$

Using (12), one can show that the variance of the angular distribution reduces to zero, by considering the limit of the second order moment as $\|\Omega_o\| \rightarrow \infty$. The second-order moment with $\cos \gamma$ being the random variable is given by:

$$\begin{aligned} \mathbb{E}[\cos \gamma - \mathbb{E}[\cos \gamma]]^2 &= e^{-\|\Omega_o\|^2/\sigma^2} \left(2\sqrt{2}\|\Omega_o\|^2\sigma^2 - \sqrt{2}e^{\|\Omega_o\|^2/\sigma^2} \pi \left(-\|\Omega_o\|^4 + 2\|\Omega_o\|^2\sigma^2 + (\|\Omega_o\|^2 - \sigma^2)^2 \right. \right. \\ &\quad \times \left. \left. \text{Erf} \left[\frac{\|\Omega_o\|}{\sqrt{2}\sigma} \right]^2 \right) + 2e^{\|\Omega_o\|^2/2\sigma^2} \|\Omega_o\| \sqrt{\pi} \sigma \left(2(-\|\Omega_o\|^2 + \sigma^2) \text{Erf} \left[\frac{\|\Omega_o\|}{\sqrt{2}\sigma} \right] \right. \right. \\ &\quad \left. \left. + \pi \sigma^2 \text{Erfi} \left[\frac{\|\Omega_o\|}{\sqrt{2}\sigma} \right] \right) \right) / \sqrt{2}\|\Omega_o\|^4 \pi. \end{aligned} \quad (13)$$

The limit of the above function of $(\|\Omega_o\|, \sigma)$ as $\|\Omega_o\| \rightarrow \infty$ converges to zero, which confirms the prementioned argument and validates the practicality of the proposed model.

A special case of angular distribution under the examined 3-D model is obtained when the amplitude of the vector Ω_o is set to zero, corresponding to the situation in which the scatter cluster is centered at the observation point. Under this assumption, the joint distribution in (4) attains a simpler form, from which it is trivial to show that the condition of isotropy applies,

$$\begin{aligned} f(\vartheta, \varphi) &= \int_0^\infty f(\|\Omega_{\rho_1, sc}\|, \vartheta, \varphi) dr = \int_0^\infty \frac{\|\Omega_{\rho_1, sc}\|^2}{(2\pi)^{3/2} \sigma^3} e^{-\|\Omega_{\rho_1, sc}\|^2/2\sigma^2} \sin \vartheta dr \\ &= \frac{\sin \vartheta}{(2\pi)^{3/2} \sigma^3} \frac{\sqrt{\pi} \sigma^3}{\sqrt{2}} = \frac{\sin \vartheta}{4\pi}. \end{aligned} \quad (14)$$

Fig. 4 HERE

The logarithmic scale of the derived angular density provides a good match with the observations made in [18]. Therein, Andersen and Pedersen illustrate an identical density in angle of arrival to the logarithmic scale of the density depicted in Fig. 4.

A. On the Conditioning of the Joint Distribution Function

In this section, the conditioning of the joint spectrum at a particular distance is examined and as shown the angular distribution is always vMF distributed. Bounding the distance variable to an infinitesimal interval is equivalent to projecting the scatterers on the surface of the sphere of radius r . This translates

to observing the distribution of angles at a particular distance, e.g. $\|\Omega_r\|$, in which case the joint density function in (4) may be expressed as the product of the conditional PDF at the particular value $\|\Omega_r\|$ and the marginal PDF of $f(\|\Omega_r\|)$. In accordance with the above and after some algebraic manipulation, the conditioned PDF may be written as follows:

$$\begin{aligned} f(\vartheta, \varphi | \|\Omega_r\|) &= \frac{f(\|\Omega_r\|, \vartheta, \varphi)}{f(\|\Omega_r\|)} \\ &= \frac{\|\Omega_r\| \|\Omega_o\| / \sigma^2}{4\pi \sinh(\|\Omega_r\| \|\Omega_o\| / \sigma^2)} e^{\|\Omega_r\| \|\Omega_o\| / \sigma^2 [\sin \vartheta \sin \vartheta_o \cos(\varphi - \varphi_o) + \cos \vartheta_o \cos \vartheta]} \sin \vartheta. \end{aligned} \quad (15)$$

Hence, the conditional density obeys the vMF distribution with concentration parameter κ given by [19]:

$$\kappa = \|\Omega_r\| \|\Omega_o\| / \sigma^2. \quad (16)$$

This important result suggests that starting from a Gaussian distribution of scatterers, the AoA spectrum conditioned at a particular distance value $\|\Omega_r\|$ will always be vMF distributed. This may be explained by recalling that the vMF distribution can be obtained by appropriate conditioning of suitable bivariate Gaussian distributions [20]. To show the effect of increasing $\|\Omega_r\|$, consider the following limit:

$$\lim_{\|\Omega_r\| \rightarrow +\infty} f(\vartheta, \varphi | \|\Omega_r\|) = \frac{1}{4\pi} \delta = \delta. \quad (17)$$

Therefore, the distribution reduces to a Dirac-Delta function as $\|\Omega_r\| \rightarrow \infty$. The angle subtended by the scatter cluster to a random point in space is clearly dependent on their intrinsic distance. In this respect, the value of σ characterizing the spread of scatterers around the mean direction vector Ω_o is not a true indicator of the angular spread. This realization, essentially distinguishes the effect of σ between the marginal distribution of distances and the conditional distribution of angles, since the range of angles is restricted to a smaller surface patch or equivalently angular interval for the 2-D case. The aforementioned line of argument allows the treatment of the parameter σ in a separate manner, and in fact in one that lies within the statistical literature of directional variables. Herein, to characterize the change in angular spread as observed at an arbitrary distance $\|\Omega_r\|$ the following formulae is proposed:

$$\kappa = \frac{\|\Omega_r\|^2}{\sigma^2}, \quad (18)$$

where κ defines the dispersion of the scatter cluster. Increasing the observation distance $\|\Omega_r\|$, increases the concentration of angles reflected through the parameter κ or equivalently decreases the dispersion around the mean vector as this is expressed through σ . Therefore, when increasing the mean vector $\|\Omega_o\|$ it is this ratio that is of interest and not the parameter σ alone. The relationship in (18) may be obtained considering

the conditioning of the angular distribution on a particular distance value, namely $f(\vartheta, \varphi | \|\Omega_r\|)$. As shown earlier, the vMF model always applies with concentration parameter $\kappa = \|\Omega_r\| \|\Omega_o\| / \sigma^2$. This allows us to substitute $\|\Omega_o\| = \|\Omega_r\|$ and proceed in order to obtain (18). In view of this analysis, the effect of restricted angular spread along the direction of interest (due to an increase in the distance between the observation unit and the scatter cluster) can be simulated by the appropriate modification of the parameters in (4). To conclude, geometrically it is inaccurate to simulate an angular power field by distributions that are defined strictly on the circumference (von Mises) of the circle [21] or on the surface of the sphere (vMF) [17]. Hence, statistical fitting and estimation should preferably take account of this knowledge, essentially treating distance as a random variable.

VI. TRANSFORMING DISTANCE INTO POWER

In this section, the concept of a power based scattering response is developed. The authors' motivation originates from the fact that the information captured by the amplitudes of the vectors in the distribution of distances, does not reveal the true power received along them. Therefore, modeling the dependency of power and distance is essential. In the following, perfect isotropic radiators with equal sensitivity in the angular domain are assumed, with the primary interest being the conversion of the distant angular spectrum into a power angular scattering response. This clearly necessitates the use of a transformation function. In the sequel, the distribution of distances near to the mobile is assumed to be Nakagami (as detailed in the previous sections), which is representative of a macrocellular scenario, with the scatterers being relatively close to the receiver as opposed to the transmitter. Derivation of the PASR when distances to scatterers are Gaussian distributed (corresponding to micro-, pico-cell scenario) is left for future work.

To derive the power received in each angular element at the receiver, the power captured by each scatterer should be found. Therefore, a hypothetical transmitter is placed in the direction of vector Ω_d , whose length determines the distance between the transmitter and receiver. In accordance with the macrocell assumption, $\Omega_c \gg \Omega_o$, where Ω_c is the vector connecting the transmitter to the CoG of the scatter cluster (see Fig. 1). The power extracted at the scatter cluster is equivalent to

$$\rho_e = \alpha / \|\Omega_{\rho_2, sc}\|^2, \quad (19)$$

and sets the basis of our transformation function, with α accounting for transmit power, gain of the antenna, scattering cross sectional area and possibly other losses. As a result of the small ratio (Ω_c/σ), a

Gaussian distribution of distances provides a good fit⁴ in this instance. Let us assume that the parameters of the Gaussian distribution are $\|\Omega_{\rho_2,sc}\| \sim N(\Omega_c = 10, \sigma = 3)$. The geometrical arrangement is illustrated in Fig. 1. It is important to clarify that this approach assumes that the mean distances to the scatterer cluster from the transmitter and the receiver are known and independent of each other, i.e., we are in the independent scenario as defined in Section II.

As shown in the preceding sections, for a large mean distance the distribution of distances tends to Gaussian. Equation (19) advises us that the power diminishes with the square of the distance (in its simplest form). Therefore, the square of the Gaussian distances should be obtained. It is trivial to show that if $\|\Omega_{\rho_2,sc}\|$ is a Gaussian random variable then $W = \|\Omega_{\rho_2,sc}\|^2$ has the density function given by (20), that is akin in functional form to the well known chi-square distribution with one degree of freedom ($k = 1$). The full derivation is omitted in here, while simply expressing the squared distances from the transmitter to the scatterer cluster by the following PDF:

$$f_W(w) = \frac{1}{2C\sqrt{2\pi}\sigma\sqrt{w}} e^{-(\sqrt{w}-\mu)^2/2\sigma^2}, \quad (20)$$

where C is a normalization constant given by, $C = 1/2 (1 + \text{Erf} [\mu/\sigma\sqrt{2}])$. Subsequently, to transform the distance distribution into a power distribution extracted at the scatter cluster, equation (19) is re-written as follows:

$$\varrho_e = \frac{\alpha}{w} \Rightarrow w = \frac{\alpha}{\varrho_e}, \quad (21)$$

whose derivative with respect to the variable ϱ_e is given by

$$\frac{dw}{d\varrho_e} = -\frac{\alpha}{\varrho_e^2}. \quad (22)$$

After substitution of (21) into (20) and making use of the above derivative, the transformed power with respect to $\|\Omega_{\rho_2,sc}\|^2$ at the scatter cluster is obtained:

$$f(\varrho_e) = f_W(w) \left| \frac{dw}{d\varrho_e} \right| = \frac{\alpha}{\varrho_e^2 (C) 2\sqrt{2\pi}\sqrt{\alpha/\varrho_e}\sigma} e^{-(\sqrt{\alpha/\varrho_e}-\mu)^2/2\sigma^2}. \quad (23)$$

The evaluation of the above probability density function for various values of ϱ_e is reported in Fig. 5. The distribution behaves identically to the Inverse-Gamma (IG), which may be shown by taking a random sample from (23) and measuring its fit using the Kolmogorov-Smirnov test. Due to the very accurate fit provided by the IG in this instance, the distribution in (23) whose density form is not known to the

⁴This statement is valid as shown in the preceding sections since larger mean distances satisfy the condition of large ratio $\|\Omega_o\|/\sigma$ set as a prerequisite for the observance of a Gaussian distribution.

authors will be approximated with an $\text{IG} \sim (\alpha_2, \beta_2)$. The fit becomes evident in Fig. 5.

Fig. 5 HERE

Following the same guidelines, a derivation for the power received at the receiving unit is now provided. The power received at ϱ_1 can be expressed as a function of the distances from the scatterer cluster to the receiver using the following relationship:

$$P_r = \beta \frac{P_e}{Y}, \quad (24)$$

where constant β accounts for the antenna gain and effective aperture, and random variable Y represents the square of the distance between a random scatterer and the receiver. Herein, it is known that ϱ_e follows the distribution in (23), i.e. approximately an Inverse Gamma distribution. Furthermore, since scatterer distances to receiver are assumed to be Nakagami distributed, the random variable Y has a Gamma distribution with parameters $(k = \bar{\mu}, \theta = \omega/\bar{\mu})$. The ratio of these two random variables results in the third random variable of interest. The problem of estimating the distribution of the ratio between two random variables can be approached by observing that $P_e/Y = P_e \times (1/Y)$. Since Y is Gamma distributed, the $1/Y$ ratio follows an inverse Gamma distribution with known parameters, i.e. $1/Y \equiv \Xi \sim \text{IG}(\alpha_1 = k, \beta_1 = \theta^{-1})$. The problem has essentially been reduced to finding the distribution of the product of two inverse gamma random variables.

To begin, let $\Psi = P_e \Xi$ and introduce a new random variable $\Phi = \Xi$. The joint density may be expressed as follows:

$$f_{\Psi, \Phi}(\psi, \phi) = f_{P_e}(\varrho_e) f_{\Xi}(\xi)/\phi = f_{P_e}(\psi/\phi) f_{\Xi}(\phi)/\phi. \quad (25)$$

The above function after integration directly leads to the desired marginal density:

$$\begin{aligned} f_{\Psi}(\psi) &= \int_0^{\infty} \frac{1}{\phi} f_{P_e}(\psi/\phi) f_{\Xi}(\phi) d\phi = \int_0^{\infty} \frac{1}{\phi} \left(\frac{\beta_1^{\alpha_1} \beta_2^{\alpha_2}}{\Gamma[\alpha_1] \Gamma[\alpha_2]} \left(\frac{\psi}{\phi} \right)^{-\alpha_1-1} e^{-\frac{\beta_1 \psi}{\phi}} \phi^{-\alpha_2-1} e^{-\frac{\beta_2}{\phi}} \right) d\phi \\ &= 2\beta_1^{\alpha_1} \beta_2^{\alpha_2} \psi^{-1-\alpha_1} \beta_2^{\alpha_1-\alpha_2/2} \left(\frac{\beta_1}{\psi} \right)^{\frac{-\alpha_1+\alpha_2}{2}} \mathbf{K}_{-\alpha_1+\alpha_2} \left(2\sqrt{\beta_2} \sqrt{\beta_1/\psi} \right), \end{aligned} \quad (26)$$

where $\psi = \varrho_r$. Therefore, the product of two inverse gamma random variables produces another inverse gamma random variable with different parameters. The evaluation of (26) appears in Fig. 6. The fit of the derived and proposed model in a practical scenario becomes evident by comparison with the angular delay histogram estimated in [9]. The authors therein proposed the use of an exponential decay function, however the theoretical analysis of this work suggests that the inverse Gamma distribution may provide a better fit. The direct comparison is allowed (power-time) due to the linear relationship between the two

transformation functions.

To conclude, it is this density jointly with the angular density, that shall form the so-called power angular scattering response. To complicate things further, in a clusterized environment the numbers of spatial clusters need not be one, where it becomes necessary to model the spatial domain as a mixture of distributions with a power prior weight defining each component's contribution to the overall power received.

Fig. 6 HERE

VII. ANGULAR POWER SCATTERING RESPONSE AND POWER AZIMUTH ELEVATION SPECTRUM

A. Expected power conditioned on angle

In the last section of this work, a novel methodology for the estimation of the angular power spectrum in the wireless propagation environment is provided. More specifically, the expected power received along each angle under the 3-D Gaussian scattering setup is derived. Our methodology begins by revealing the nature of the conditional distribution of distances in each angular element ϑ, φ . Considering the joint distribution (4), and by division with the angular distribution in (11) over the whole radial space, one obtains the following:

$$\begin{aligned} f(\|\mathbf{\Omega}_r\| | \vartheta, \varphi) &= \frac{f(\|\mathbf{\Omega}_r\|, \vartheta, \varphi)}{f(\vartheta, \varphi)} \\ &= \frac{2\|\mathbf{\Omega}_r\|^2}{\sigma} e^{-(2\|\mathbf{\Omega}_o\|^2 + \|\mathbf{\Omega}_r\|^2 - 2\|\mathbf{\Omega}_r\|\|\mathbf{\Omega}_o\|\cos\gamma)/2\sigma^2} \left(2\|\mathbf{\Omega}_o\|\sigma\cos\gamma + \right. \\ &\quad \left. + e^{\|\mathbf{\Omega}_o\|^2\cos^2\gamma/2\sigma^2} \sqrt{2\pi} (\sigma^2 + \|\mathbf{\Omega}_o\|^2\cos^2\gamma) \left(1 + \text{Erf} \left[\frac{\|\mathbf{\Omega}_o\|\cos\gamma}{\sqrt{2}\sigma} \right] \right) \right). \end{aligned} \quad (27)$$

The derived density, defining distance density conditioned on a specific angular sector, closely resembles the initially derived distribution of distances, with the dependency being shifted to the angular domain. More specifically, as the angle increases in the $(0, \pi]$ interval, this distribution obtains an asymmetric shape, while from $(\pi, 2\pi]$ the distribution becomes symmetric in the mean. Transforming the conditional distribution of distance into power and obtaining the expectation of each conditional distribution results in a Gaussian-like angular power spectrum in each angle. The Gaussian APS/PAS was also proposed in [22]. Additionally, the PAS estimated from measurements in Stockholm and Aarhus in [18] may serve as another indication of a Gaussian PAS observed in practice. The superiority of the derived 3-D PAS against the Laplacian PAS in [9] lies not only in its fit to measurements, but also on the theoretical framework from which it arises. In fact, a Laplacian spectrum does not have a well-defined theoretical basis.

B. Angular scattering response with path powers

The PASR as defined in this work denotes the product of the true scattering response $f(\|\mathbf{\Omega}_{\rho_1,sc}\|, \vartheta, \varphi)$ with the antenna response $g(\vartheta, \varphi; \vartheta_o, \varphi_o)$, whose maximum radiation points towards ϑ_o, φ_o . In this work, the PASR is constructed without considering the effect of directionality of the antenna response, and therefore equal sensitivity has been explicitly assumed in all directions. Assuming isotropic antennas in these derivations is also useful since it allows a fair comparison between the presented material and those of measurement campaigns, in which the effect of antenna pattern is eliminated through proper calibration. A realistic antenna response will give rise to a pattern-weighted angular power scattering response or angular power spectrum. The pattern-weighted angular power scattering response can be integrated in the spatial correlation formulae developed in [23], where obtaining the spherical harmonic coefficients of the impinging field becomes the primary objective.

To continue along the research lines of this section, note that this methodology follows from fact that the joint spectrum in (4) may be written independently in terms of powers and angles. Accordingly, the received PASR may be expressed by the following product:

$$f(\varrho_r, \vartheta, \varphi) = f(\varrho_r) \times f(\vartheta, \varphi; \|\mathbf{\Omega}_o\|, \sigma) \quad (28)$$

Fig. 7 HERE

The PASR derived according to (28) is reported in linear scale in Fig. 7 and logarithmic (dB) scale in Fig. 8. The logarithmic scale reveals an important point with respect to other observations made in practice [9], [18]. A Gaussian scattering distribution in space gives rise to a Gaussian angle of arrival, an inverse Gamma power distribution and a Gaussian angular power density function. The above holds also under path loss models characterized by a path loss exponent larger than 2, as assumed in this paper. Note that the second lobe in Fig. 8, which was not visible in linear scale, indicates the probability of receiving power from the direction opposite to the array's look direction. This is in accordance with the assumption that the receiver is located in the close-in region, where the Nakagami distribution of scattering distances applies. Under this assumption (recall Fig. 3), the probability of having scatterers located "backward" in the direction to the scatterer cluster is non-negligible, and gives rise to the small power density observed in the secondary lobe of the PASR.

Summarizing, it has been shown that the derived 3-D PASR is Gaussian; the usefulness of this result

lies in the fact that antenna correlation is not solely dependent on the average PAS, but the instantaneous response as well, which can be sampled using the model presented herein.

Fig. 8 HERE

VIII. WORK SUMMARY

In this paper, a novel 3-D geometric stochastic model has been developed, based on the well known 3-D Gaussian density function for scatterers. Derivations are presented for the angular and distance domains. As shown in the paper, the probability densities in power and angle provide a good fit with other measurement-based results reported in the literature. The proposed model allows the construction of a 3-D angular power scattering response, which accounts for the power-distance dependency. Under the assumption of free-space propagation, the Gaussian scattering assumption results in a Gaussian angular power density and a Gaussian angular power spectrum. The same method could be extended for any transformation function presenting the current state-of-the-art path loss models. As shown, conditioning the joint spectrum at any value of distance results in a von-Mises Fisher spectrum in the angular domain, although a different notion of concentration must be used to fully capture concentration of angles around the mean direction. Furthermore, the distribution of distances to scatterers is shown to exhibit a Nakagami shape in the close-in region, and a Gaussian shape for further distances. The foreseeing target of this work has been the simulation of the antennas response under a realistic and well-defined power angular field. The proposed model can be applied for the optimization of the antenna response in order to minimize the correlation experienced between the elements. This essentially offers some degree of pattern diversity to the system by orthogonalizing the embedded patterns.

REFERENCES

- [1] M. B. Knudsen and G. F. Pedersen, "Spherical outdoor to indoor power spectrum model at the mobile terminal," *IEEE J. Sel. Areas Commun.*, vol. 20, no. 6, pp. 1156–1169, Aug. 2002.
- [2] M. Toeltsch, J. Laurila, K. Kalliola, A. F. Molisch, P. Vainikainen, and E. Bonek, "Statistical characterization of urban spatial radio channels," *IEEE J. Sel. Areas Commun.*, vol. 20, no. 3, pp. 539–549, Apr. 2002.
- [3] K. B. Baltzis and J. N. Sahalos, "A simple 3D geometric channel model for macrocell mobile communication," *Wireless Pers. Commun.*, vol. 51, no. 2, pp. 329–347, 2008.
- [4] S. J. Nawaz, B. H. Qureshi, and N. M. Khan, "A generalized 3D scattering model for macrocell environment with directional antenna at BS," *IEEE Trans. Veh. Technol.*, vol. 59, no. 7, pp. 3193–3204, Sep. 2010.
- [5] R. Janaswamy, "Angle of arrival statistics for a 3-d spheroid model," *IEEE Trans. Veh. Technol.*, vol. 51, no. 5, pp. 1242–1247, 2002.
- [6] A. Kuchar, J. P. Rossi, and E. Bonek, "Directional macro-cell channel characterization from urban measurements," *IEEE Trans. Antennas Propag.*, vol. 48, no. 2, pp. 137–146, Feb. 2000.
- [7] J. Fuhl, J. P. Rossi, and E. Bonek, "High-resolution 3-D direction-of-arrival determination for urban mobile radio," *IEEE Trans. Antennas Propag.*, vol. 45, no. 4, pp. 672–682, Apr. 1997.
- [8] K. Kalliola, H. Laitinen, P. Vainikainen, M. Toeltsch, J. Laurila, and E. Bonek, "3-D double-directional radio channel characterization for urban macrocellular applications," *IEEE Trans. Antennas Propag.*, vol. 51, no. 11, pp. 3122–3133, Nov. 2003.
- [9] K. I. Pedersen, P. E. Mogensen, and B. H. Fleury, "A stochastic model of the temporal and azimuthal dispersion seen at the base station in outdoor propagation environments," *IEEE Trans. Veh. Technol.*, vol. 49, no. 2, pp. 437–447, Mar. 2000.

- [10] Q. H. Spencer, B. D. Jeffs, M. A. Jensen, and A. L. Swindlehurst, "Modeling the statistical time and angle of arrival characteristics of an indoor multipath channel," *IEEE J. Sel. Areas Commun.*, vol. 18, no. 3, pp. 347–360, Mar. 2000.
- [11] R. Janaswamy, "Angle and time of arrival statistics for the Gaussian scatter density model," *IEEE Trans. Wireless Commun.*, vol. 1, no. 3, pp. 488–497, Jul. 2002.
- [12] R. B. Ertel and J. H. Reed, "Angle and time of arrival statistics for circular and elliptical scattering models," *IEEE J. Sel. Areas Commun.*, vol. 17, no. 11, pp. 1829–1840, Nov. 1999.
- [13] A. Papoulis, *Probability, Random Variables and Stochastic Processes*. McGraw-Hill, 1991.
- [14] M. Abramowitz and I. A. Stegun, *Handbook of Mathematical Functions*, Dover, 1964.
- [15] J. D. MacKay, *Information Theory, Inference, and Learning Algorithms*. Cambridge University Press, 2005.
- [16] K. Mammassis and R. W. Stewart, "The Fisher-Bingham spatial correlation model," *IEEE Trans. Veh. Technol.*, vol. 58, no. 5, pp. 2130–2136, 2009.
- [17] —, "Spatial fading correlation model using mixtures of vMF distributions," *IEEE Trans. Wireless Commun.*, vol. 8, no. 4, pp. 2046–2055, Apr. 2009.
- [18] J. B. Andersen and K. I. Pedersen, "Angle-of-arrival statistics for low resolution antennas," *IEEE Trans. Antennas Propag.*, vol. 50, no. 3, pp. 391–395, Mar. 2002.
- [19] K. V. Mardia, *Statistics of Directional Data*. Academic Press, 1972.
- [20] K. V. Mardia and P. E. Jupp, *Directional Statistics*. John Wiley & Sons, 2000.
- [21] A. Abdi, J. A. Barger, and M. Kaveh, "A parametric model for the distribution of the angle of arrival and the associated correlation function and power spectrum at the mobile station," *IEEE Trans. Veh. Technol.*, vol. 51, no. 3, pp. 425–434, May 2002.
- [22] F. Adachi, M. Feeny, W. A. Williamson, and J. Parsons, "Crosscorrelation between the envelopes of 900 mhz signals received at a mobile radio base station site," *IEE Proceedings Communications, Radar and Signal Processing*, vol. 133, no. 6, pp. 506–512, Oct. 1986.
- [23] P. D. Teal, T. D. Abhayapala, and R. A. Kennedy, "Spatial correlation for general distributions of scatterers," *IEEE Signal Process. Lett.*, vol. 9, no. 10, pp. 305–308, Oct. 2002.

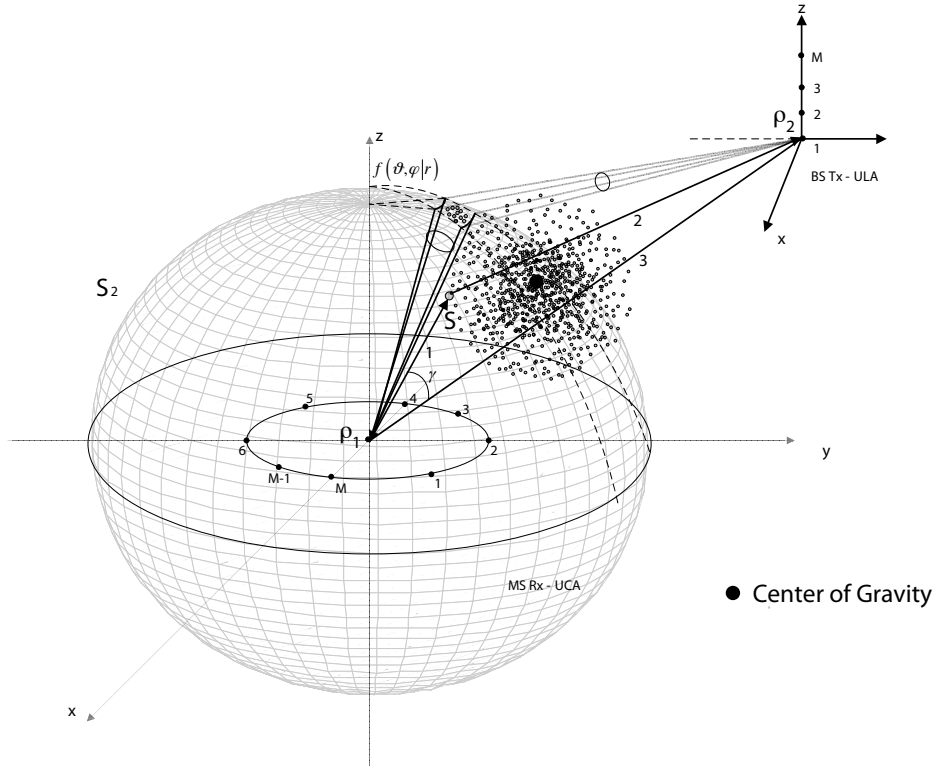
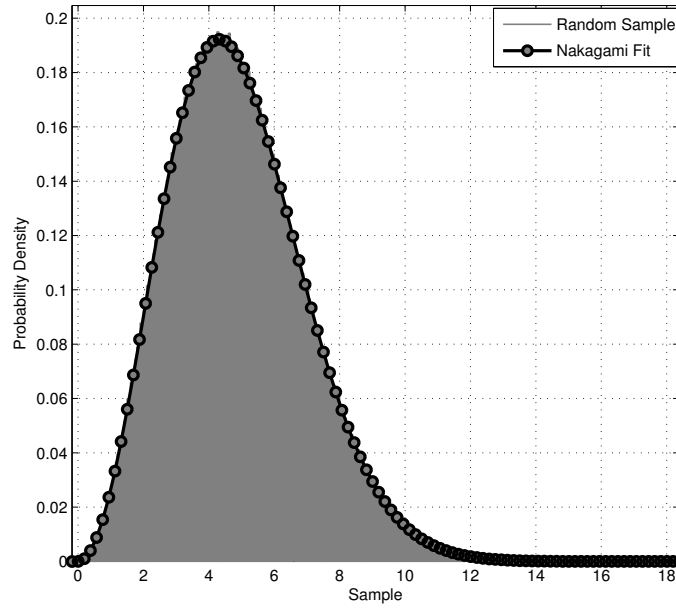
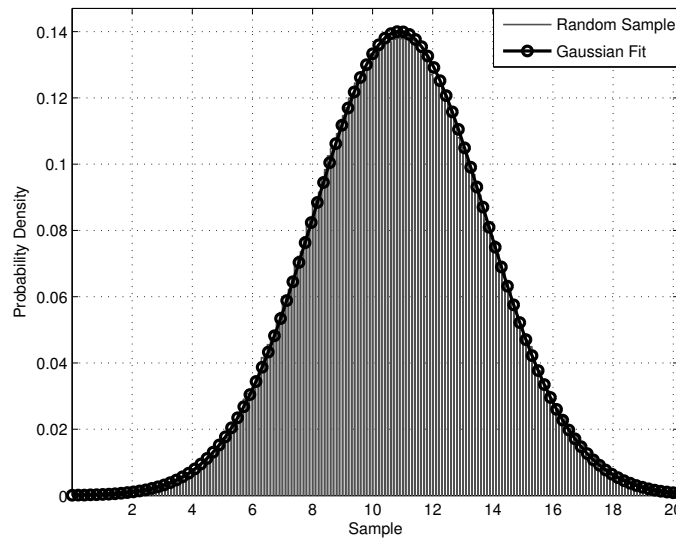


Fig. 1: This figure shows a cluster of scatterers Gaussianly distributed in x, y, z around a CoG located at (x_0, y_0, z_0) . Note that the vector denoted as 1 is indicative of the distance between the receiving point and a scatterer, i.e. $\|\Omega_{\rho_1,sc}\|$. Similarly, vector 2 indicates the transmitter to scatterer distance $\|\Omega_{\rho_2,sc}\|$. Vector 3 represents the distance between receiver ρ_1 and transmitter ρ_2 , and is denoted Ω_d . The figure also illustrates the case where the scatterers are conditioned on a particular value of $f(\|\Omega_r\|)$, hence equidistance from ρ_1 is preserved. This makes the scatterers located directly on the surface of the sphere.



(a) Nakagami distribution fit to random sample of a mean distance $\|\Omega_o\| = 1$.



(b) Gaussian distribution fit to random sample of a mean distance $\|\Omega_o\| = 10$.

Fig. 2: Goodness-of-fit of a Nakagami and Gaussian distributions for small and large mean distance respectively. The standard deviation σ of the scatter distribution is set to 3.

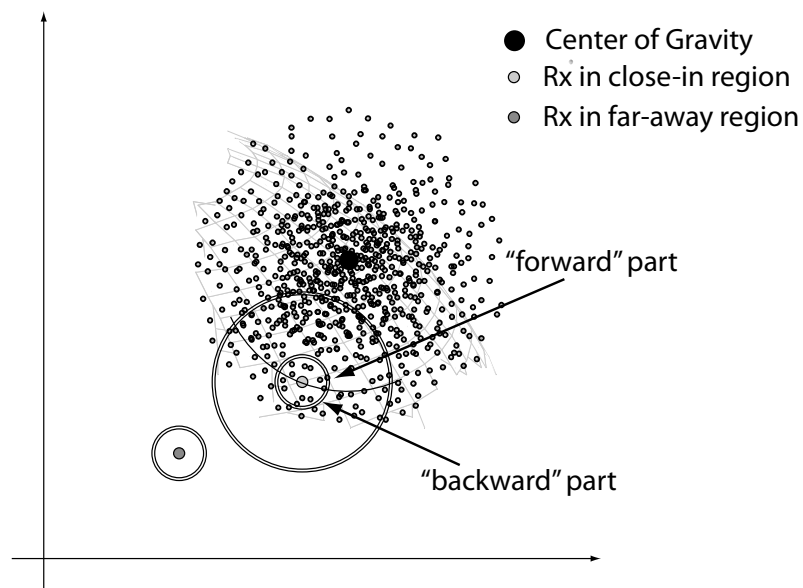
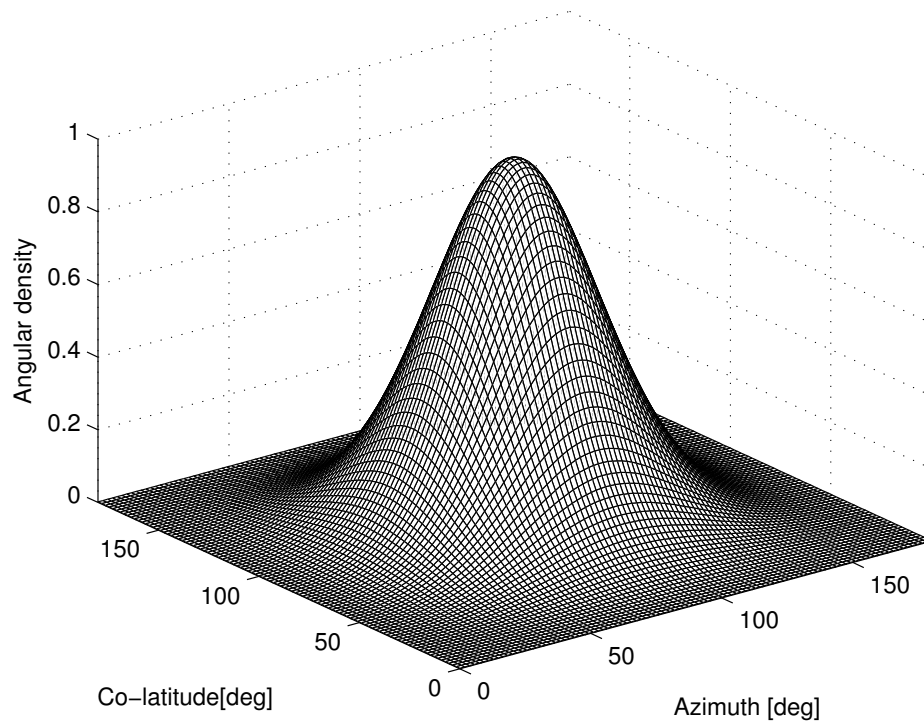
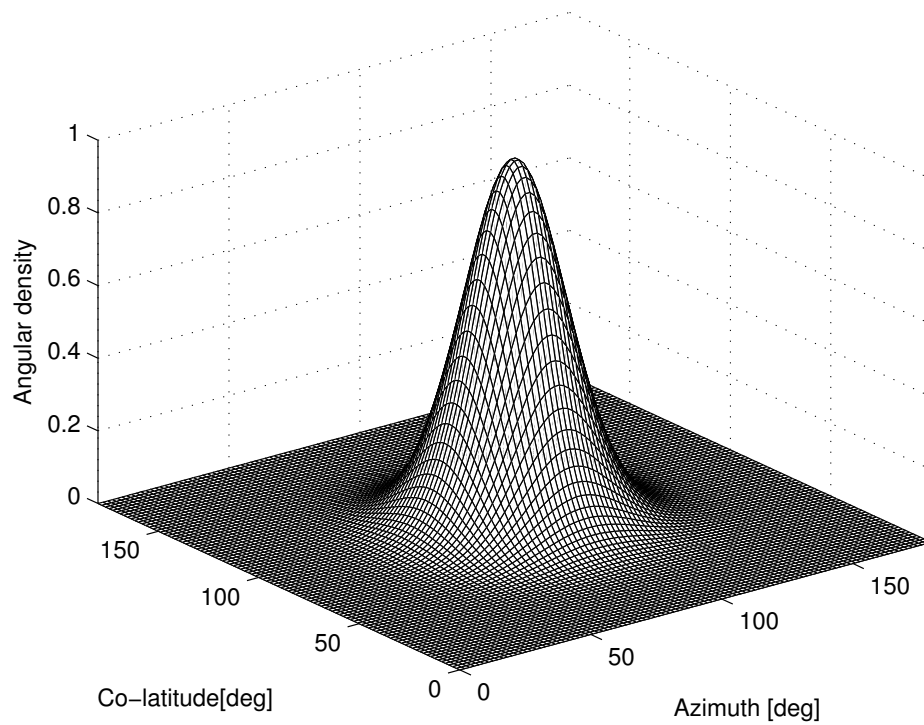


Fig. 3: Graphical explanation of the left-skewness observed in distance distribution when the observation point is in the close-in region (light shaded disk). When the observation point lies in the far-away region (dark shaded disk), the distance distribution is symmetric.

(a) $\|\Omega_o\| = 5$.(b) $\|\Omega_o\| = 10$.Fig. 4: Effect of increasing $\|\Omega_o\|$ in the concentration of angles.

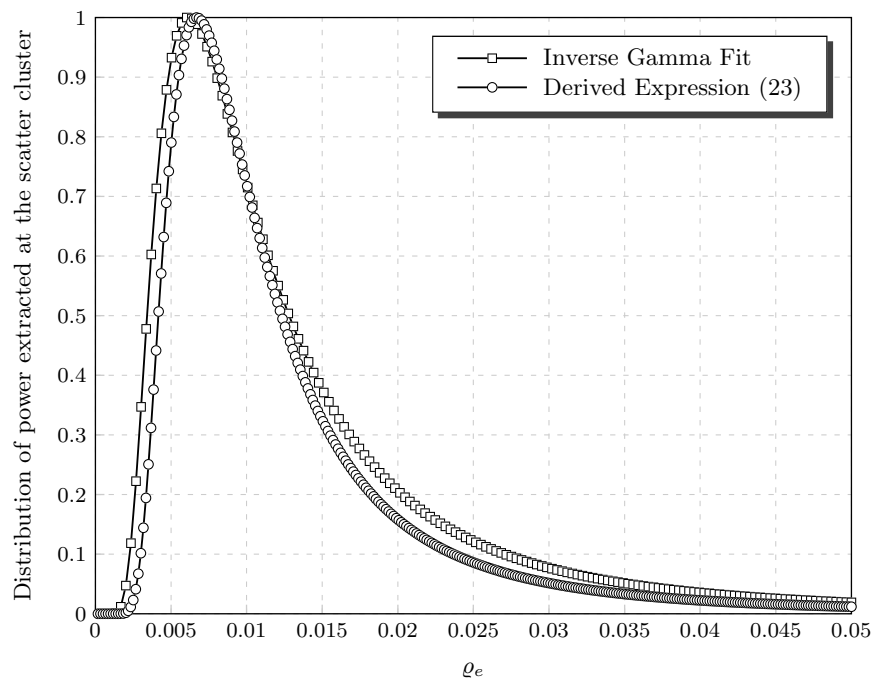


Fig. 5: This figure illustrates the probability density of power $f(\rho_e)$ as dictated by $f_W(w)$ at the scatter cluster, and the goodness of fit of the Inverse-Gamma distribution (with parameters $\alpha_2 = 2.25, \beta_2 = 0.02$) to the PDF derived in (23). The Kolmogorov-Smirnov test statistic was not rejected at 5% significance level.

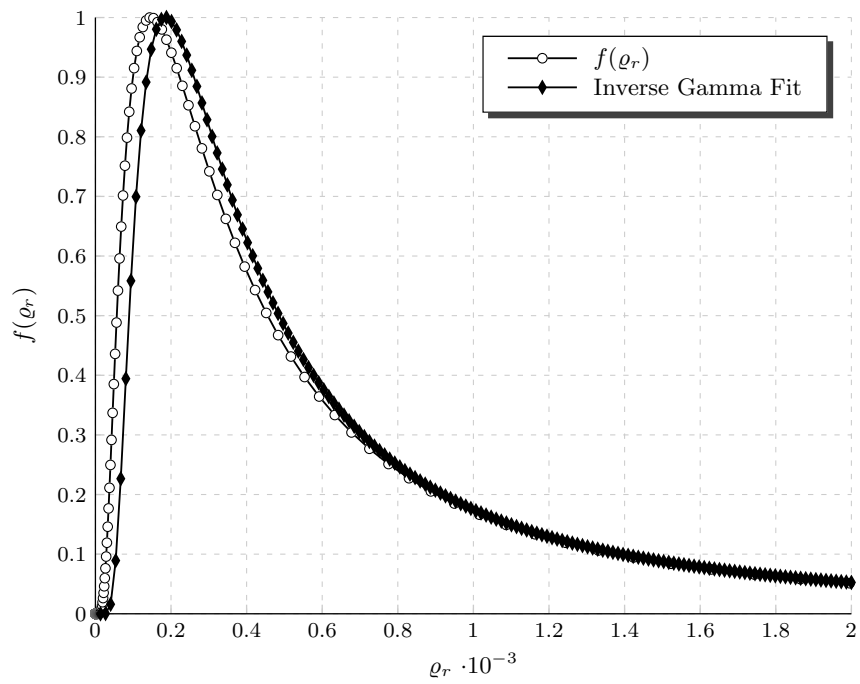


Fig. 6: Evaluation of the derived power density function at the receiver. The distribution can be accurately approximated by an Inverse Gamma distribution with parameters $\alpha_3 = 1, \beta_3 = 0.00037$. Note that the inverse Gamma fit of the power distribution has been verified in the corresponding histogram estimated in [9].

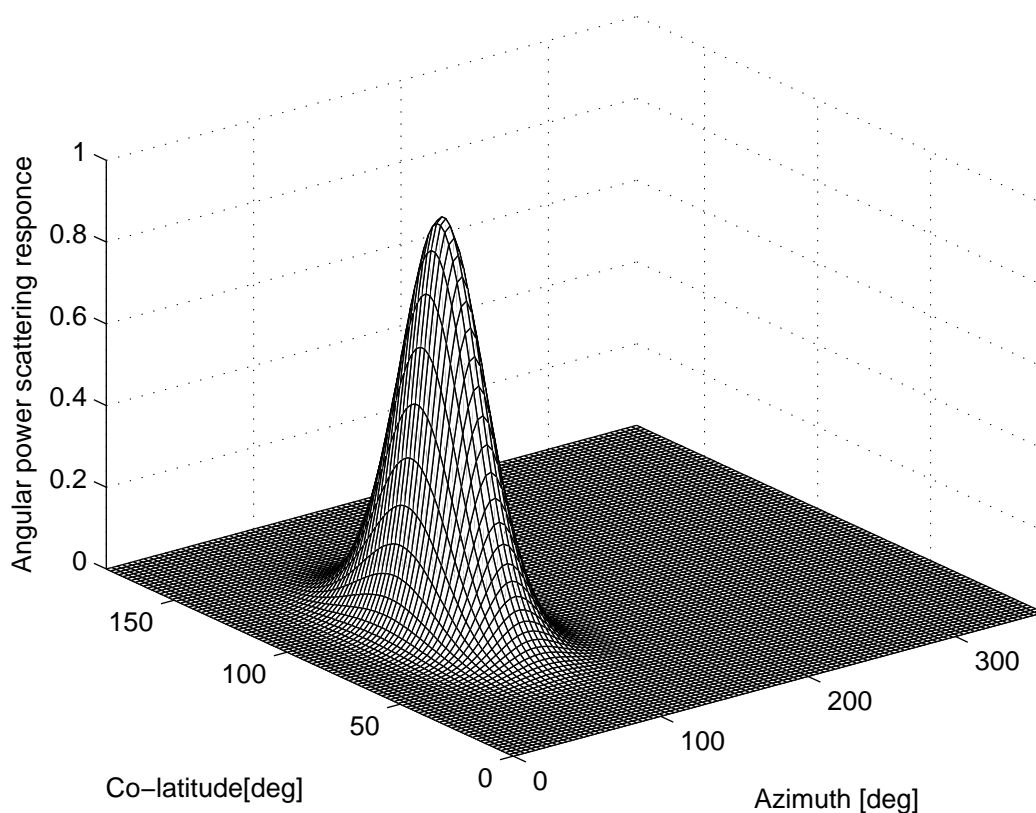
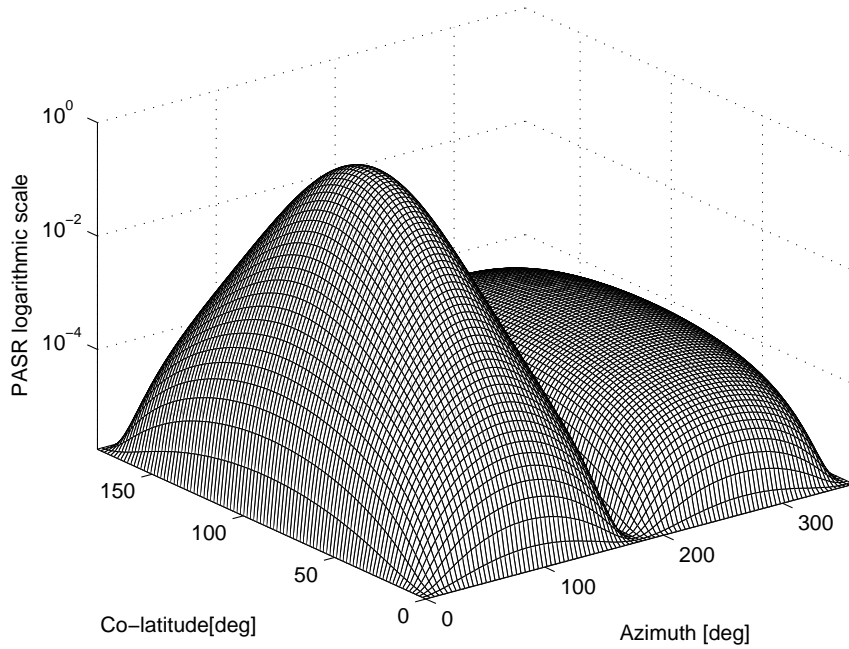
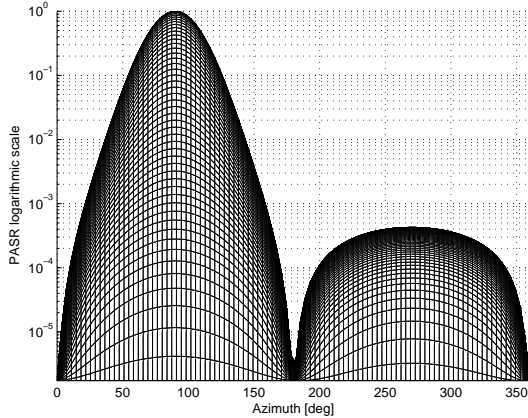


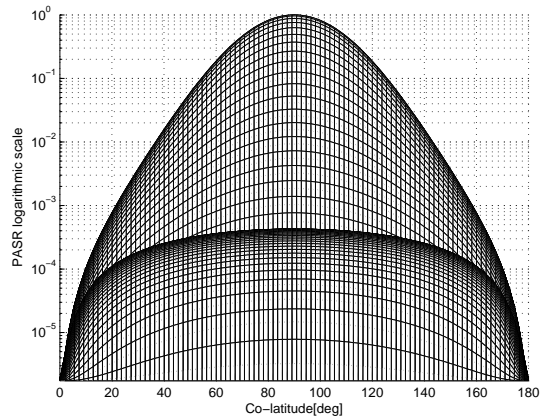
Fig. 7: In this figure, the derived power angular scattering response in (28) is illustrated as a function of azimuth and elevation. The plot was generated for a mean azimuthal and elevation angle of 90 degrees. Note that the 3-D density is conditioned on a particular value of power/distance, since otherwise the plot would be in four dimensions and hence graphically unobtainable.



(a) Logarithmic scale of the power angular scattering response in (28).



(b) Azimuthal view of spectrum.



(c) Co-latitude view of spectrum.

Fig. 8: The three figures provided show sequentially the angular power spectrum of the Gaussian 3-D model in all view directions. The azimuthal view suggests a very good fit between the derived model and the model fit through measurements in [9], while the co-latitude view possesses an identical shape due to Gaussian symmetry. The second lobe observed in the azimuth power spectrum is determined from the position of the receiver, which in this case is assumed to be located in the close-in region, where the Nakagami distance distribution provides a good fit. At remote distances, the power received in the second lobe diminishes to zero as is the case in [9].